Connecting the Simpler Structures to Topologically Close-Packed Phases

Anirudh Raju Natarajan and Anton Van der Ven

Phys. Rev. Lett. **121**, 255701 — Published 17 December 2018

DOI: 10.1103/PhysRevLett.121.255701

Connecting the simpler structures to topologically close-packed phases

Anirudh Raju Natarajan* and Anton Van der Ven†
Materials Department, University of California, Santa Barbara
(Dated: October 25, 2018)

Pathways connecting dissimilar crystal structures are fundamental to our understanding of structural phase transitions. In this letter we report on a new pathway connecting the hexagonal closed packed crystal structure to a hierarchy of topologically close-packed phases consisting of Kagomé and triangular nets. Common intermetallic structure prototypes such as the Friauf-Laves phases, $CaCu_5$, Ce_2Ni_7, Be_3Nb and Co_7Gd_2 are specific members of this hierarchy. We find that the pathway is facile for compounds with large atomic size differences, which has implications for the nucleation mechanism of these complex phases.

Phase transformations connecting vastly different crystal structures are ubiquitous in pure elements and multicomponent crystals and are exploited in shape-memory[1–6], magnetocaloric[7, 8] and precipitation strengthened alloys[9, 10]. The structural pathways between different crystal structures are a cornerstone of our understanding of common phase transformations in the solid state. Nevertheless, despite almost a century of research on structural phase transitions, only a handful of crystallographic pathways linking a few simple crystal structures are known.

The Bain path[11] links the bcc (body centered cubic) and fcc (face centered cubic) crystal structures through a homogeneous tetragonal deformation of their cubic unit cells. The bcc and hcp (hexagonal close packed) structures can be connected through the Burgers path[12], which combines a macroscopic shape change with an internal atomic shuffle within the hcp unit cell. Pathways have also been identified connecting the hcp and bcc crystal structures to the slightly more complex ω phase, made up of alternating triangular and honeycomb layers [13–15]. Pathways connecting bcc to a family of close-packed "R" phases and to the B19' phase are also known[1, 3–6].

While the structural transformations involving hcp, bcc, fcc, ω and other close-packed phases are well understood, a majority of the crystal structure prototypes that are commonly observed in alloys remain disconnected. The topologically close-packed (TCP) Frank-Kasper phases [16, 17], for example, are an especially common[18] class of crystal structures that form in alloy systems whose end members adopt the simpler fcc, hcp and bcc crystal structures [19, 20]. There are many distinct structures that fall into this class of compounds, with the Friauf-Laves phases being the most common and well studied. Many compounds that form topologically close-packed crystal structures display exotic electronic, magnetic and mechanical phenomena[21–29]. Icosahedral arrangements of atoms similar to the Frank-Kasper compounds are also observed in glasses and liquids[30–32]. Frank-Kasper phases are not restricted to metallic alloys, but have also shown promise as photonic crystals [33] and have been observed to form during the crystallization of block co-polymers and colloidal self-assembly [34–38].

In this letter, we identify a family of new transformation pathways that link a major subset of the Frank-Kasper phases to simpler close packed structures. We show that a simple two-dimensional rearrangement of the triangular lattice can be used to build a series of hierarchical phases starting with the simple close-packed hcp crystal structure. Structures like the Laves phases, $CaCu_5$, Ce_2Ni_7, Be_3Nb and Co_7Gd_2 structure prototypes are found to be specific members of this hierarchy. Furthermore, we show that the pathways that link the close-packed structures to the TCP phases are facile and will occur spontaneously for particular arrangements of close packed atoms that have very different atomic volumes.

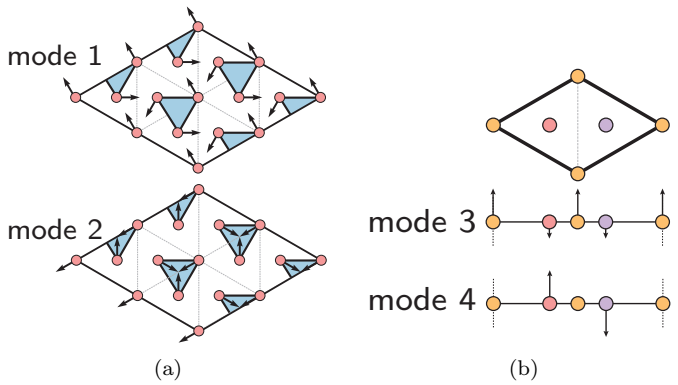

FIG. 1. Symmetry-adapted distortion modes on a $\sqrt{3} \times \sqrt{3}$ supercell of the triangular lattice: (a) Connects the triangular lattice to the Kagomé net (b) dissociates a triangular layer into three separate triangular layers with one atom in each layer. The SI contains a mathematical description of these modes[39]

The Friauf-Laves phases and related crystal structures can be viewed as stackings of Kagomé nets interleaved by triangular layers [16, 17]. We start by showing how the Kagomé nets and triangular layers of the Laves phases can be formed by a superposition of symmetry adapted collective displacements of the triangular close-packed layers of hcp.

The collective displacements have the periodicity of a $\sqrt{3}a \times \sqrt{3}a$ supercell of the primitive cell of the tri-

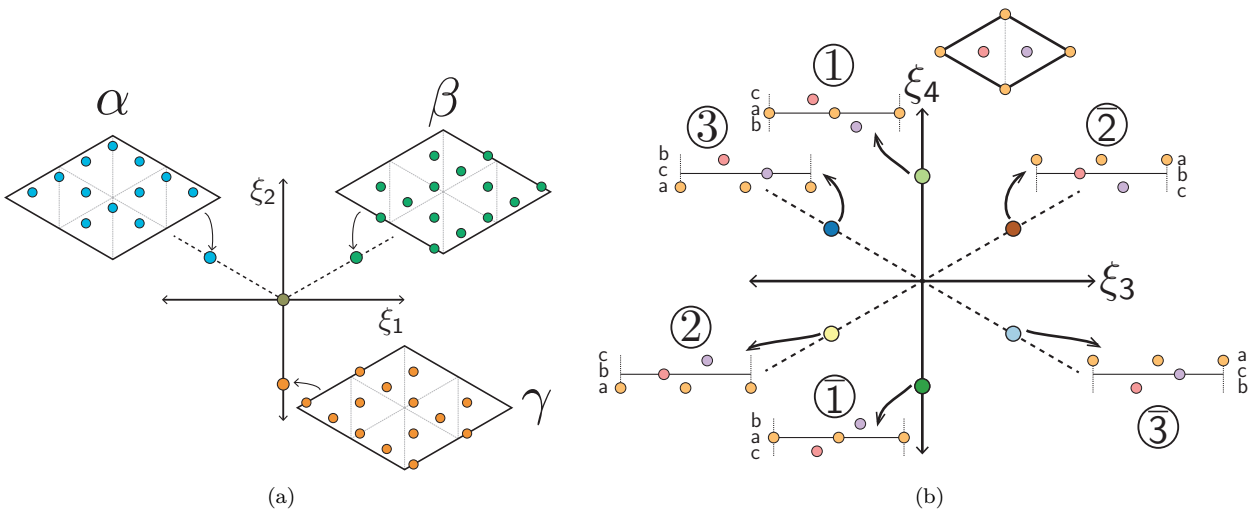

FIG. 2. (a) Amplitudes of symmetry-adapted distortion modes on a triangular lattice that connect them to the Kagomé net (b) Six translational variants of a vertically split triangular lattice.

angular lattice (where a is the lattice parameter). Figure 1a shows two symmetry-adapted collective displacements that link a triangular lattice to a Kagomé net. The collective displacements are easily understood when considering the periodically repeating triplet clusters on the triangular lattice illustrated in fig. 1a. The first collective distortion, with amplitude ξ_1, displaces atoms tangentially relative to the centers of the periodically repeating triplet clusters. The second collective distortion, with amplitude ξ_2, corresponds to a dilation of the periodically repeating triplet clusters of sites. Three translational variants of the Kagomé net can be generated from the triangular lattice in the space spanned by ξ_1 and ξ_2. A negative value of ξ_2 generates one Kagomé net, that we label γ. The two other Kagomé nets, α and β, can be generated by a combination of ξ_1 and ξ_2 residing on the dashed lines in fig. 2a that are rotated by -120^o and 120^o relative to the negative ξ_2 axis.

Out of plane collective displacements having the translational periodicity of the $\sqrt{3}a \times \sqrt{3}a$ supercell can be defined that split a triangular lattice into three parallel triangular lattices with an "abc" stacking, each having one third of the sites of the original triangular lattice. Six translational variants of a vertically split triangular lattice can be generated with two symmetry adapted collective displacements. One collective displacement with amplitude ξ_3 moves two atoms within a $\sqrt{3}a \times \sqrt{3}a$ supercell down and the third atom up as illustrated in fig. 1b. The other collective displacement with amplitude ξ_4 "dissociates" the layer, in that one of the atoms in the $\sqrt{3}a \times \sqrt{3}a$ supercell moves up, another moves down and the third atom remains fixed. The six translationally equivalent split configurations reside on a hexagon in ξ_3-ξ_4 space as illustrated in fig. 2b.

The collective distortions illustrated in figs. 1a and 1b can be used to generate a hierarchy of crystal structures starting from hcp that consist of different stackings of Kagomé nets and triangular layers. The hierarchy can be generated by converting the A layers of an ABAB stacked hcp crystal to a Kagomé net upon activation of the $\xi_1 - \xi_2$ distortion amplitudes of fig. 2a, and by dissociating a subset of the B layers into three new triangular layers by activating the $\xi_3 - \xi_4$ amplitudes. The particular distortion of each A layer will be represented with t, α, β, γ, where t refers to the undistorted layer, and the other three letters correspond to the Kagomé variants. The dissociation of the B layer will be represented as $1, 2, 3, \overline{1}, \overline{2}, \overline{3}$ as shown in fig. 2b, with the undistorted layer denoted as 0. With this notation the hcp structure becomes "$t0$".

The first generation of hierarchical phases derived from hcp is $\{\alpha 0\}$. $\alpha 0$ consists of identical Kagomé nets generated from the A layers interleaved by undissociated triangular B layers. The resulting crystal structure corresponds to the $CaCu_5$ prototype. The second generation results in crystal structures that are periodic over four layers and include: $\{t0\alpha 0, \alpha 2\gamma\overline{2}\}$. The first member can be formed by combining the zeroth generation (i.e. hcp) with the first generation. The second distortion, $\alpha 2\gamma\overline{2}$, is new, and results in the formation of the well-known C14-$MgZn_2$ Laves crystal structure.

Several other well-known structure prototypes appear at higher generations. Examples are listed in table I. The two other Laves phase prototypes emerge as distortions in the third and fourth generations. The structure prototypes Ce_2Ni_7, Be_3Nb and Co_7Gd_2 form in the sixth and ninth generations. Table I shows that the structural distortions of fig. 2a and fig. 2b are capable of connecting a significant fraction of common intermetalllic compounds to hcp. Similar relationships may be drawn between hcp

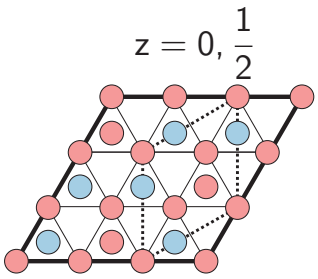

FIG. 3. Ordering on hcp related to $MgZn_2$ (C14). The atoms shown in red are the smaller majority specie, while the blue atoms are the minority specie. Atoms on a grid point are in the A layer while atoms in the middle of a triangle are on the B layer.

and structures such as the σ and μ phases. However, these transformations are slightly more complicated as they require additional interstitial atoms.

Structure Prototype	Structure Label
$CaCu_5$	$\alpha 0$
$MgZn_2$ (C14)	$\beta 1 \gamma \overline{1}$
$MgCu_2$ (C15)	$\beta 1 \gamma \overline{2} \alpha 3$
$MgNi_2$ (C36)	$\beta 1 \gamma \overline{1} \beta \overline{3} \alpha 3$
Ce_2Ni_7	$\beta \overline{3} \alpha 0 \alpha 0 \alpha 3 \beta 0 \beta 0$
Be_3Nb	$\alpha 2 \gamma 0 \beta 1 \gamma 0 \gamma \overline{2} \alpha 0$
Co_7Gd_2	$\alpha 0 \alpha 3 \beta 0 \beta 0 \beta 1 \gamma 0 \gamma 0 \gamma \overline{2} \alpha 0$

TABLE I. Known crystal structure prototypes their corresponding labels within the family of structures that can be derived from hcp.

Most topologically close-packed phases are compounds containing two or more chemical species. The majority element X is usually smaller than the minority element Y, with both having strong site preferences within the crystal structure of the topologically close-packed phase. There are, therefore, very specific orderings in the precursor hcp phase that result in different topologically close-packed phases upon application of the distortions of fig. 2a and fig. 2b. Figure 3 illustrates the decoration of Mg and Zn on an hcp crystal structure that is necessary to form perfect $MgZn_2$ having the C14 crystal structure. The triangular layer of hcp that converts to a Kagomé net only contains the smaller Zn atoms (i.e. X) while the other layer that dissociates into three new triangular layers contains two Mg atoms (i.e. Y) for every Zn atom. The precursor ordering in hcp has a $\sqrt{3}a \times \sqrt{3}a$ super cell on the triangular lattice. Inspection of known topologically close-packed phases reveals that the precursor hcp layers that transform into a Kagomé net will invariably only consist of the smaller X. The layers that dissociate or remain triangular, are found to be either pure X or exhibit a similar $\sqrt{3}a \times \sqrt{3}a$ ordering of X and Y as in the precursor hcp phase of $MgZn_2$ illustrated in fig. 3.

First-principles electronic structure[40] calculations

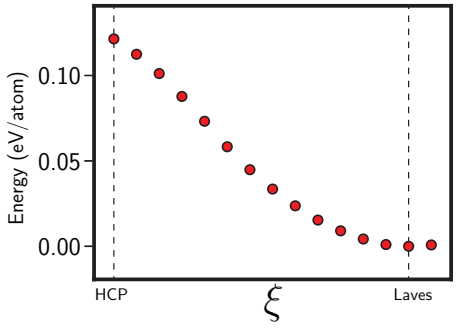

FIG. 4. Energy landscape along the path connecting the ordering of fig. 3 to C14 in the Mg-Zn binary alloy.

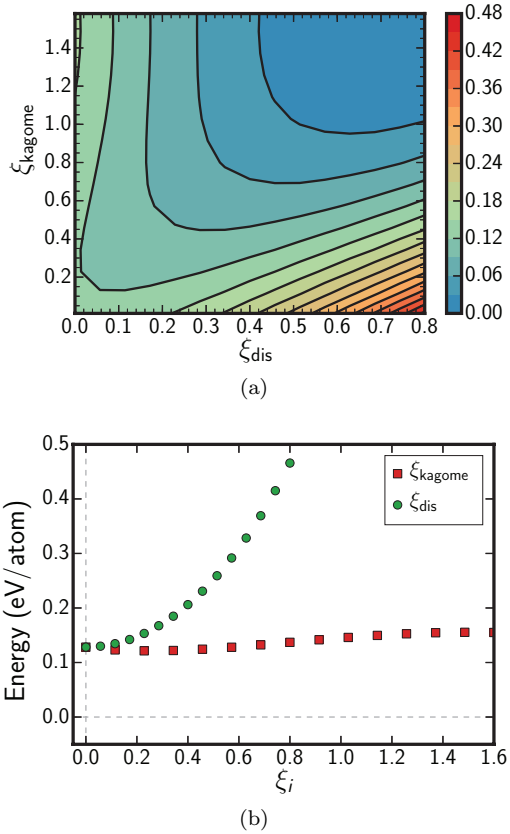

FIG. 5. Energy landscape connecting the hcp crystal structure with the C14 Laves phase in Mg-Zn. (a) Energy as a function of the dissociative and Kagomé modes. (b) Sections of the energy landscape showing that the hcp structure is unstable with respect to a transformation towards Kagomé nets.

can reveal how facile the pathways described above are. Figure 3 shows the Mg-Zn ordering in the hcp precursor phase. It is evident from fig. 4 that there is no barrier separating the two crystal structures, with the hcp form of $MgZn_2$ being dynamically unstable. Any local ordering on hcp that is similar to fig. 3 will experience a driving force to spontaneously collapse into C14-$MgZn_2$.

Figure 5a shows the energy as a function of an amplitude $\xi_{\text{Kagomé}}$ that converts the A layers of hcp $MgZn_2$

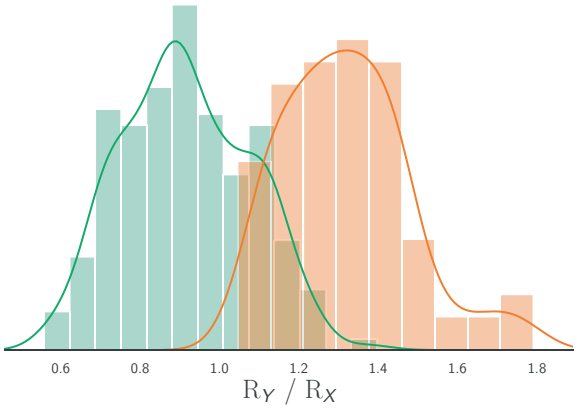

FIG. 6. Density distributions of X_2Y orderings on hcp that are stable in hcp (green) and collapse to form the C15 Laves phase (orange) across a range of chemistries and radius ratios. Metallic radii are used for each element[39, 41].

(consisting only of Zn) into Kagomé nets and a second amplitude ξ_{dis} that dissociates the B layers (consisting of Mg and Zn in a 2:1 ratio) into three new triangular layers. As is clearly revealed by fig. 5a a combination of both $\xi_{\text{Kagomé}}$ and ξ_{dis} is necessary to achieve the steepest descent from hcp to C14. However, fig. 5b, which plots the energy as a function of either $\xi_{\text{Kagomé}}$ or ξ_{dis}, shows that distortions along ξ_{dis} do not lead to an instability of the hcp crystal. Rather, it is a distortion of the A layer to form Kagomé nets that induces the spontaneous formation of the Laves phase. This can be attributed to the size mismatch between the Mg and Zn atoms. The larger Mg atoms reside in the B layers of hcp and require the formation of Kagomé nets containing large hexagonal openings before they can dissociate upwards and downwards. The formation of the Kagomé nets are essential to reduce the overcrowding that exists when arranging two species with very different sizes within the close-packed hcp crystal structure.

The instability of hcp with respect to a spontaneous collapse to a Laves phase is not restricted to $MgZn_2$, but is predicted to occur quite uniformly among a large number of X_2Y compounds when Y is substantially larger than X. We investigated the stability of 511 X_2Y compounds in the hcp crystal structure with respect to a spontaneous collapse to C15 with DFT (for more details on the chemistries of these compounds see SI[39]). Figure 6 shows normalized histograms of the compounds that remain stable in hcp and those that spontaneously collapse to C15, plotted as a function of the ratio of the metallic radii[41] of Y and X, i.e. R_Y/R_X. As is clearly revealed by fig. 6, compounds with large R_Y/R_X radius ratios are found to undergo a barrierless structural phase transition to C15 when ordered on hcp, while those with smaller radius ratios are stable in hcp. There is some overlap between the two distributions around $R_Y/R_X \approx 1.1$, however, a large number of these compounds consist of refractory elements, which are likely to adopt radii within compounds that differ from their metallic radii due to charge transfer [42]. As shown in the SI [39], the qualitative trends of fig. 6 remain unchanged when using different definitions for the atomic radii[43, 44]. These results suggest that atoms with large size mismatch are unlikely to order on close-packed parent crystal structures due to the facile pathways discovered here that will convert hcp into the more favorable Frank Kasper phases.

The discovery of the Bain and Burgers paths almost a century ago played a crucial role in rationalizing a large number of phase transformations in the solid state. The facile crystallographic pathways reported here will similarly enable a deeper understanding of phase transformation mechanisms between close-packed structures and Frank-Kasper phases, which rank among the most common structures adopted by intermetallic compounds[18]. Frank-Kasper phases have traditionally been viewed as crystallographically very distinct from the common close-packed structures. We have demonstrated that hcp can be converted into a large number of the Frank-Kasper phases with minimal structural distortions. This facile pathway suggests that the nucleation of Frank-Kasper phases within supersaturated hcp solid solutions does not require large structural rearrangements but rather can occur coherently and in a continuous manner. Composition and ordering fluctuations within the hcp parent crystal structure can enable the formation of local precursor orderings, that can then collapse into a coherent nucleus of the incipient Frank-Kasper phase through a dynamical instability. Nucleation by this mechanism, while possibly accompanied by coherency strains, would bypass the need for energetically costly incoherent interfaces and will result in well defined orientational relationships, at least in the early stages when coherency strains play less of a role. A survey of binary alloy phase diagrams suggests several material systems where this mechanism may be exploited[45]. In fact, the observed orientation relationship for Laves phases in magnesium alloys[23, 46–52] ($(0001)_{\text{Laves}} \parallel (0001)_{\text{hcp}}, [1\bar{1}00]_{\text{Laves}} \parallel [11\bar{2}0]_{\text{hcp}}$) is in agreement with our prediction of the basal plane of the Laves structure being aligned with that of hcp and the $\sqrt{3}\times\sqrt{3}$ direction of hcp being along one of the basal lattice vectors of the Laves phase. Instead of treating the nucleation of Frank-Kasper phases within hcp as a singularity, as conventionally done for reconstructive phase transitions, the simple hcp to Frank-Kasper phase pathway along with the predicted instabilities of the precursor ordering within hcp suggests a continuous nucleation mechanism. These insights are expected to unlock new design routes to either encourage (or suppress) the formation of topologically close-packed phases in a wide variety of metallic, polymeric and colloidal systems.

We are grateful to Dr. Hari Kumar for helpful discus-

sions. This material is based upon work supported by the National Science Foundation, Grant DMREF-DMR-1729166. We acknowledge support from the Center for Scientific Computing from the CNSI, MRL: an NSF MRSEC (DMR-1121053). This research used resources of the National Energy Research Scientific Computing Center, a DOE Office of Science User Facility supported by the Office of Science of the U.S. Department of Energy under Contract No. DE-AC02-05CH11231.

---

* anirudh@ucsb.edu
† avdv@ucsb.edu

[1] X. Huang, G. J. Ackland, and K. M. Rabe, Nature materials **2**, 307 (2003).
[2] Y. Ogawa, D. Ando, Y. Sutou, and J. Koike, Science **3**, 30 (2016).
[3] N. A. Zarkevich and D. D. Johnson, Physical Review Letters **113** (2014), 10.1103/PhysRevLett.113.265701.
[4] K. Otsuka and X. Ren, Progress in Materials Science **50**, 511 (2005).
[5] S. Sarkar, X. Ren, and K. Otsuka, Physical Review Letters **95** (2005), 10.1103/PhysRevLett.95.205702.
[6] Y. Ji, D. Wang, X. Ding, K. Otsuka, and X. Ren, Physical Review Letters **114** (2015), 10.1103/PhysRevLett.114.055701.
[7] B. Dutta, A. Çakır, C. Giacobbe, A. Al-Zubi, T. Hickel, M. Acet, and J. Neugebauer, Physical Review Letters **116** (2016), 10.1103/PhysRevLett.116.025503.
[8] J. Liu, T. Gottschall, K. P. Skokov, J. D. Moore, and O. Gutfleisch, Nature Materials **11**, 620 (2012).
[9] T. M. Pollock, Science **328**, 986 (2010).
[10] J. H. Chen, E. Costan, M. a van Huis, Q. Xu, and H. W. Zandbergen, Science (New York, N.Y.) **312**, 416 (2006).
[11] E. Bain and N. Dunkirk, Transactions of the American Institute of Mining and Metallurgical Engineers **70** (1924).
[12] W. Burgers, Physica **1**, 561 (1934).
[13] J. C. Jamieson, Science **140**, 72 (1963).
[14] D. de Fontaine, Acta Metallurgica **18**, 275 (1970).
[15] D. R. Trinkle, R. G. Hennig, S. G. Srinivasan, D. M. Hatch, M. D. Jones, H. T. Stokes, R. C. Albers, and J. W. Wilkins, Physical Review Letters **91** (2003), 10.1103/PhysRevLett.91.025701.
[16] F. Frank and J. S. Kasper, Acta Crystallographica **11**, 184 (1958).
[17] F. t Frank and J. S. Kasper, Acta Crystallographica **12**, 483 (1959).
[18] R. Ferro and A. Saccone, *Intermetallic Chemistry* (Pergamon, 2008).
[19] A. K. Sinha, Progress in Materials Science **15**, 81 (1972).
[20] F. Stein, M. Palm, and G. Sauthoff, Intermetallics **12**, 713 (2004).
[21] J. C. Duthie and D. G. Pettifor, Physical Review Letters **38**, 564 (1977).
[22] W. Zhang, R. Yu, K. Du, Z. Cheng, J. Zhu, and H. Ye, Physical Review Letters **106** (2011), 10.1103/PhysRevLett.106.165505.
[23] H. Xie, H. Pan, Y. Ren, L. Wang, Y. He, X. Qi, and G. Qin, Physical Review Letters **120** (2018), 10.1103/PhysRevLett.120.085701.
[24] M. F. Chisholm, S. Kumar, and P. Hazzledine, Science **307**, 701 (2005).
[25] S. Khmelevskyi, P. Mohn, J. Redinger, and M. Weinert, Physical Review Letters **94** (2005), 10.1103/PhysRevLett.94.146403.
[26] J. Feng, N. W. Ashcroft, and R. Hoffmann, Physical Review Letters **98** (2007), 10.1103/PhysRevLett.98.247002.
[27] T. Matsuoka, M. Debessai, J. J. Hamlin, A. K. Gangopadhyay, J. S. Schilling, and K. Shimizu, Physical Review Letters **100** (2008), 10.1103/PhysRevLett.100.197003.
[28] A. Alam and D. D. Johnson, Physical Review Letters **107** (2011), 10.1103/PhysRevLett.107.206401.
[29] M.-C. Marinica, F. Willaime, and J.-P. Crocombette, Physical Review Letters **108** (2012), 10.1103/PhysRevLett.108.025501.
[30] D. R. Nelson and F. Spaepen, in *Solid State Physics*, Vol. 42 (Elsevier, 1989) pp. 1–90.
[31] J. Fransaer, A. V. Wagner, and F. Spaepen, Journal of Applied Physics **87**, 1801 (2000).
[32] J. Zemp, M. Celino, B. Schonfeld, and J. Loffler, Physical Review Letters **115** (2015), 10.1103/PhysRevLett.115.165501.
[33] A.-P. Hynninen, J. H. J. Thijssen, E. C. M. Vermolen, M. Dijkstra, and A. van Blaaderen, Nature Materials **6**, 202 (2007).
[34] S. Lee, C. Leighton, and F. S. Bates, Proceedings of the National Academy of Sciences **111**, 17723 (2014).
[35] C. X. Du, G. van Anders, R. S. Newman, and S. C. Glotzer, Proceedings of the National Academy of Sciences **114**, E3892 (2017).
[36] K. Kim, A. Arora, R. M. Lewis, M. Liu, W. Li, A.-C. Shi, K. D. Dorfman, and F. S. Bates, Proceedings of the National Academy of Sciences **115**, 847 (2018).
[37] S. Hajiw, B. Pansu, and J.-F. Sadoc, ACS Nano **9**, 8116 (2015).
[38] B. Cabane, J. Li, F. Artzner, R. Botet, C. Labbez, G. Bareigts, M. Sztucki, and L. Goehring, Physical Review Letters **116** (2016), 10.1103/PhysRevLett.116.208001.
[39] See Supplemental Material at [URL will be inserted by publisher] for a detailed description of the transformation pathways and calculations of the correlation between radius ratio and the onset of structural transformation. ().
[40] Total energies were calculated within the Perdew-Burke-Ernzerhof (PBE) parameterization of the generalized gradient approximation (GGA)[53] to density functional theory (DFT)[54, 55]. The *Vienna Ab-Initio Simulation Package* (VASP)[56–59] was used to relax configurations. All degrees of freedom were relaxed to test the stability of specific orderings across a range of chemistries. The energy landscape along the pathway connecting hcp to the C14 Laves phase was calculated by minimizing the energy with respect to the volume while fixing all other degrees of freedom. An energy cutoff of 600 eV was used for the plane-wave basis set. The k-point grids were chosen to contain 71 k-points per $Å^{-1}$. Structure interpolations and symmetry analysis of the pathways were carried out with the CASM[60] and ISODISPLACE[61] software packages.

[41] N. N. Greenwood and A. Earnshaw, *Chemistry of the Elements*, 2nd ed. (Butterworth-Heinemann, 1997).
[42] A. Dwight, Transactions of the American Society of Metals **53**, 479 (1961).
[43] E. Clementi, D. L. Raimondi, and W. P. Reinhardt, The Journal of Chemical Physics **47**, 1300 (1967).
[44] J. C. Slater, The Journal of Chemical Physics **41**, 3199 (1964).
[45] A survey of the Landolt-Bornstein database[62] and the ASM binary phase diagram handbook[63] suggests that the following binary alloys contain two-phase regions between a disordered hcp solid solution and a structure belonging to the family of orderings described in this study: Be-{Ag,Ti},Ca-Mg,Co-{Mg,Sc},Cr-{Hf,Ti,Zr},Hf-{Mo,V,W},Mg-Yb,Mn-{Y,Zr},Mo-Zr,Re-{Sc,Y},{V,W}-Zr.
[46] J.-F. Nie, Metallurgical and Materials Transactions A **43**, 3891 (2012).
[47] C. Mendis, K. Oh-ishi, and K. Hono, Materials Science and Engineering: A **527**, 973 (2010).
[48] B. Langelier, A. Korinek, P. Donnadieu, and S. Esmaeili, Materials Characterization **120**, 18 (2016).
[49] A. Suzuki, N. Saddock, J. Jones, and T. M. Pollock, Acta Materialia **53**, 2823 (2005).
[50] T. Homma, S. Nakawaki, K. Oh-ishi, K. Hono, and S. Kamado, Acta Materialia **59**, 7662 (2011).
[51] X. Gao and J. Nie, Scripta Materialia **56**, 645 (2007).
[52] T. Homma, S. Nakawaki, and S. Kamado, Scripta Materialia **63**, 1173 (2010).
[53] J. P. Perdew, K. Burke, and M. Ernzerhof, Physical Review Letters **77**, 3865 (1996).
[54] P. Hohenberg and W. Kohn, Physical Review **136**, 864 (1964).
[55] W. Kohn and L. Sham, Physical Review **140**, 1133 (1965).
[56] G. Kresse and J. Hafner, Physical Review B **47**, 558 (1993).
[57] G. Kresse and J. Furthmüller, Physical Review B **54**, 11169 (1996).
[58] G. Kresse and J. Furthmüller, Computational Materials Science **6**, 15 (1996).
[59] G. Kresse and J. Hafner, Physical Review B **49**, 14251 (1994).
[60] CASM Developers, "CASM: A Clusters Approach to Statistical Mechanics," (2016).
[61] B. J. Campbell, H. T. Stokes, D. E. Tanner, and D. M. Hatch, Journal of Applied Crystallography **39**, 607 (2006).
[62] *Londolt-Börnstein Database* (Springer).
[63] *Alloy Phase Diagrams*, 10th ed., ASM Handbook, Vol. 3 (1992).